Species comparison of liver proteomes reveals enhanced lipid metabolism, reduced mitochondrial respiration and enhanced expression of detoxifying enzymes in the long-lived naked mole-rat

Authors:

Ivonne Heinze[1*], Martin Bens[1*], Enrico Calzia[2*], Susanne Holtze[3], Oleksandr Dakhovnik[1], Arne Sahm[1], Joanna M. Kirkpatrick[1], Karol Szafranski[1], Natalie Romanov[4], Stephan Singer[5], Maria Ermolaeva[1], Matthias Platzer[1#], Thomas Hildebrandt[3#] and Alessandro Ori[1#]

[1] Leibniz Institute on Aging – Fritz Lipmann Institute (FLI), Jena, Germany
[2] Institute of Anesthesiological Pathophysiology and Process Engineering, University of Ulm, Germany
[3] Leibniz Institute for Zoo & Wildlife Research (IZW), Berlin, Germany
[4] Structural and Computational Biology Unit, European Molecular Biology Laboratory, Heidelberg, Germany
[5] Institute of Pathology, University Hospital Heidelberg, Heidelberg, Germany

[*] co-first authors
[#] co-senior authors

Correspondence should be addressed to: matthias.platzer@leibniz-fli.de or HILDEBRAND@izw-berlin.de or alessandro.ori@leibniz-fli.de

Abstract:

Mammals display wide range of variation in their lifespan. Lifespan is generally correlated to body size, but outliers such as human and the naked mole-rat (NMR, *Heterocephalus glaber*) exist. Investigating the molecular networks that distinguish long- from short-lived species has proven useful to identify determinants of longevity. Here, we compared the liver of long-lived NMRs and the phylogenetically closely related, shorter-lived, guinea pigs (GP, *Cavia porcellus*) using an integrated transcriptomic and proteomic approach. We found that NMRs express substantially higher levels (up to 30 fold) of a restricted number of longevity-associated proteins that confer enhanced buffering against oxidative stress. Moreover, NMR livers display a unique expression pattern of mitochondrial proteins that result in distinct metabolic features of their mitochondria. For instance, we observed a generally reduced respiration rate associated with lower protein levels of respiratory chain components, particularly complex I, and increased capacity to utilize fatty acids. Interestingly, the same molecular networks are affected during aging in both NMR and humans, supporting a direct link to the extraordinary longevity of both species. Finally, we used our analysis to identify novel longevity pathways, and validated one of them experimentally in the phylogenetically distantly related nematode *C. elegans.*

Introduction:

Among mammals lifespan generally correlates with other life-history parameters such as gestation period and body mass [1]. In this perspective, a subterranean rodent, the naked mole-rat (*Heterocephalus glaber,* NMR), and humans represent two species outliers by having an exceptionally long lifespan relatively to their body mass. NMRs are eusocial animals that live in colonies where only a subgroup of animals is devoted to reproduction (usually a queen and one male called pasha) [2]. NMRs exhibit other exceptional traits including lifelong fertility, resistance to infection, high regenerative capacity, resistance to cancer and diabetes, reviewed in [3,4]. For these reasons, NMRs have drawn attention of multiple studies aimed at identifying the molecular mechanisms behind their extreme longevity and resistance to age-related diseases. Comparative genome analysis has revealed positively selected genes in NMR [5,6], and RNA-seq analysis revealed minimal changes in gene expression during aging [5,7], supporting the view of enhanced maintenance of homeostasis in NMRs at the molecular level. NMRs possess enhanced protein stability and increased proteasomal activity [8,9], negligible levels of cellular senescence [10], over-activation of pathways that contribute to stress resistance (e.g., the nuclear factor erythroid2-related factor 2 (NFE2L2, previously NRF2/Nrf2) and p53) [3,11], atypical expression of extracellular matrix components, such as high molecular mass hyaluronan, that confer resistance against cancer development [12]. Intriguingly, NMRs have higher steady-state levels of oxidative damage compared to, e.g., mouse [8,13], and possess mitochondria with unusual morphology in the heart and skeletal muscle [14]. However, NMRs appear to be protected from the age-dependent increase in oxidative damage that manifest in other species [8], presumably due to enhanced detoxifying systems [15].

There is a wealth of evidence linking energy metabolism to the aging process and organism lifespan. Dietary interventions and nutrient sensing pathways have been shown to play a central role in modulating aging in different organisms [16–18]. Studies of genes under positive selection pressure across related species that show different lifespan have highlighted genes involved in mitochondrial homeostasis balance [19], likely influencing both energy metabolism and hormetic responses affecting lifespan [20]. Age-dependent changes of mitochondrial ultrastructure and activity have been described both in flies and mice [21].

There is emerging evidence that metabolic changes in the NMR contribute to adaptation to its ecosystem [22], allow to act as a "superorganism" with its eusocial life style [4], and might be related to its extreme longevity. However, the relationship between NMR metabolism and longevity has not yet been investigated. Given its central role in organism metabolism, we set out to investigate the liver of NMRs in order to identify novel molecular signatures of longevity. Since ecological adaptations are more likely to affect gene expression (Fraser 2013), and mechanisms of aging act both at the transcript and protein level [23], we performed a cross-species comparison between NMR and the shorter-lived guinea pig (*Cavia porcellus,* GP) using an integrated proteomic and transcriptomic approach. In order to investigate cross-species differences in the

context of aging, we additionally analyzed livers from young and old NMRs, and related the identified changes to human aging by studying the liver proteome of 12 individuals aged between 31 and 88 years. Finally, we validated one of the newly identified longevity pathways to be a mediator of lifespan in the nematode *C. elegans.*

Results:

Cross-species comparison of liver proteomes reveals elevated expression of detoxifying enzymes in naked mole rats

We first compared the liver proteomes of 4 young adult male NMRs (2.7-3.8 year old (yo)) and GPs (0.7-1 yo) using mass spectrometry (Table S1). For each animal, we obtained a quantitative proteome profile by liquid chromatography tandem mass spectrometry, and estimated absolute protein abundances using the iBAQ method [24]. In order to directly compare the two species, we mapped both NMR and GP proteins to the respective human orthologs, and used these as the reference for comparison (see Material and Methods). This allowed us to perform a quantitative comparison of the two species using estimated absolute abundances for 3248 protein groups quantified by at least two unique proteotypic peptides in both species (Figure 1A and Table S2). In order to validate our approach, we obtained RNA-seq data from the same samples and determined transcript-level fold changes between the two species. For this, only those reads that exclusively mapped to conserved regions were used, a method used for transcriptomic cross-species comparisons [7] (Table S2). Protein and transcript fold changes displayed a significant positive correlation (Pearson $R=0.52$, $p<2.2e-16$, Figure 1B), which is in line with comparisons performed within the same species [25]. These data indicate that our strategy can reveal meaningful differences in protein abundance between species and that many of these changes are driven by changes in transcript levels.

We next asked whether our comparison would reveal known longevity-associated proteins. We found strikingly higher levels of peroxiredoxin 1 (PRDX1) and thioredoxin reductase 1 (TXNRD1) in NMRs as compared to GPs (Figure 1C and D). *PRDX1* and *TXNRD1* are both target genes of the transcription factor NFE2L2, they play a crucial role in maintaining cell redox homeostasis, and both have been shown to influence lifespan in multiple species by buffering ROS and promoting proteostasis [26–28]. Interestingly, both PRDX1 and TXNRD1 are cytosolic enzymes, and their mitochondrial counterparts (PRDX5, TXNRD2) are instead expressed at similar levels in both species (Table S2).

We next wondered whether we could identify similar differences in other organs. For this purpose, we compared RNA-seq data from heart, skin, kidney and cerebellum across the two species and found that increased transcript levels of *PRDX1* occur exclusively in the liver (Figure 1E and F). This suggests that increased level PRDX1 and TXNRD1 might be linked to a specific metabolic activity of the NMR liver.

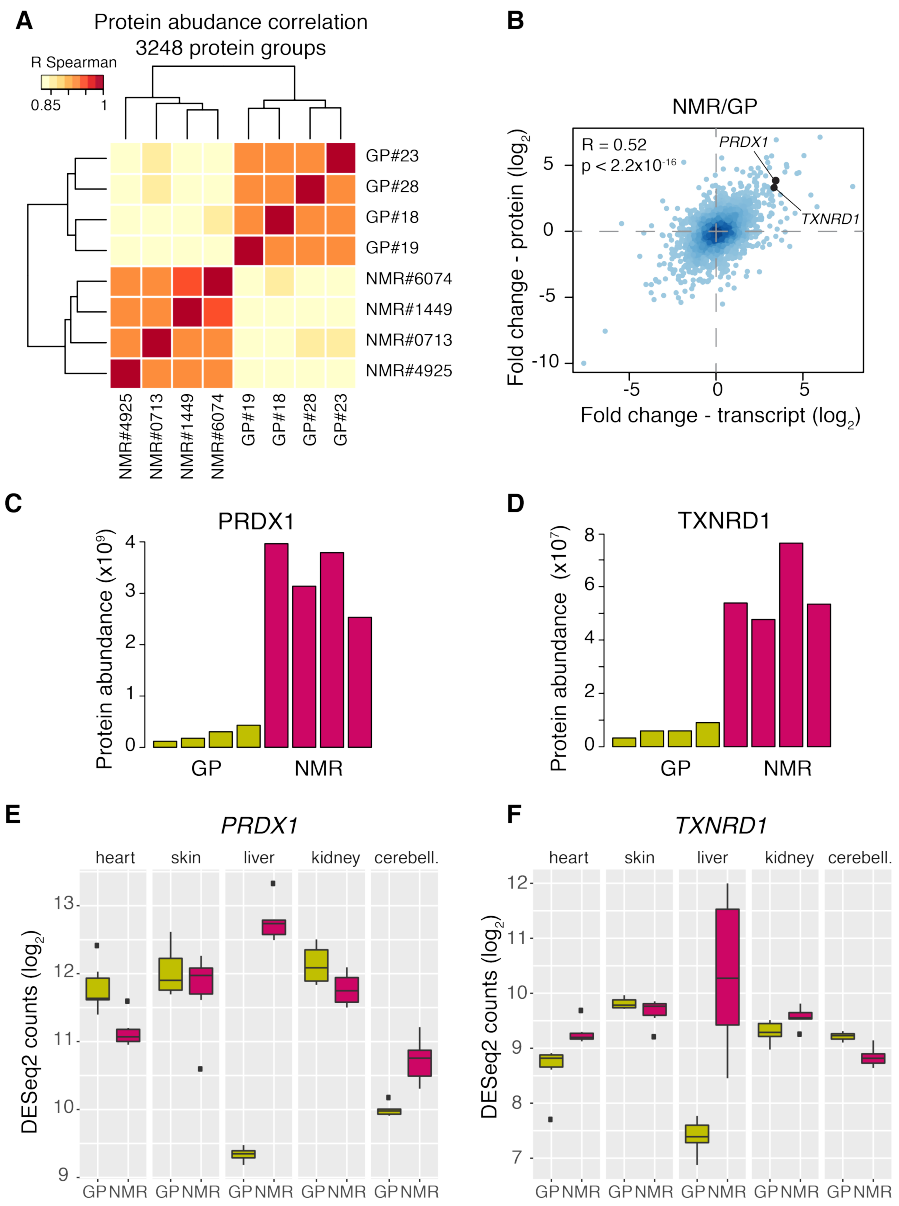

Figure 1. Cross-species comparison of the liver proteome integrated with RNA-seq from the same animals. (A) Liver proteomes from 4 adult naked mole rats (NMRs) and 4 guinea pigs (GPs) were compared using quantitative mass spectrometry. Hierarchical clustering based on the correlation between proteome profiles based on 3248 protein groups quantified across the two species. **(B)** Correlation between fold changes estimated at the protein level by quantitative mass spectrometry and at the transcript level by RNA-seq. For RNA-seq analysis only reads mapping to conserved regions between the two species were considered. **(C and D)** PRDX1 and TXNRD1 as examples of longevity-associated proteins that show drastically increased abundance in NMR vs. GP. Each bar represents the abundance estimated for one animal. **(E and F)** Comparison of transcript levels of *PRDX1* and *TXNRD1* across multiple tissues. For both genes, transcript levels are increased in NMR vs. GP in the liver ($q<2.2x10^{-300}$ for *PRDX1*; $q=1.5x10^{-45}$ for *TXNRD1*), while they show similar abundances in the other tissues examined. Related to Tables S1 and S2.

The liver of naked mole rats has a unique metabolism characterized by reduced mitochondrial respiration and enhanced lipid metabolism

Intrigued by this finding, we used gene set enrichment analysis to investigate differences in pathways and molecular networks between the long-lived and shorter-lived species. Our analysis returned pathways linked to energy metabolism (Figure 2A and Table S3). In particular, we found pathways related to lipid metabolism to be up regulated, and gene sets related to oxidative phosphorylation to be down regulated in NMR ($q<0.05$). Among up-regulated proteins involved in lipid metabolism, we found enzymes responsible for fatty acid beta-oxidation (e.g., ACOX2 and ACOX3), and lipid (e.g., ACACA and ACSL5), cholesterol (e.g., MVD and DHCR24) and bile acids biosynthesis (e.g., AMACR) compared to GP (Figure 2A and B and Table S2). Many of these are direct target of the nuclear receptor peroxisome proliferator-activated receptor alpha (PPARα), a master regulator of energy metabolism linked to aging [29] (Figure 2B). The majority of these enzymes showed higher abundance in the liver of NMRs both at transcript and protein level, irrespectively of their sub-cellular localization (Figure 2B).

In order to exclude that such differences would arise from a different organelle composition of the NMR liver cells, we analyzed the distribution of fold changes for proteins belonging to different cell compartments and found slight, but significantly lower general levels of mitochondrial proteins (mean $\log_2$ fold change=-0.17, p=0.01, Welch two sample t-test), and higher levels of lysosomal proteins (mean $\log_2$ fold change=0.2, p=0.005, Welch two sample t-test) in NMR compared to GP.

Regarding oxidative phosphorylation, NMRs showed reduced abundance of a subset of mitochondrial respiratory chain components (Figure 2C). Interestingly, these differences manifested almost exclusively at the protein level, and affected to different extents the respiratory chain complexes, with components of complex I being the most strongly reduced (mean $\log_2$ fold change=-1.53, $p=7.2\times10^{-5}$, Welch two sample t-test, Figure 2D). The opposite changes of mitochondrial enzymes involved in lipid metabolism and respiratory chain components indicate that NMR livers possess a distinct composition of their mitochondrial proteome.

In order to investigate whether proteomic differences result in altered mitochondrial activity of NMR liver parenchyma, we performed *ex vivo* measurements of cellular respiration in liver extracts of NMR by means of high-resolution respirometry (see Material and Methods). We measured mitochondrial respiration from an independent group of adolescent (1 yo, n=4) and mature adult (10 yo, n=4) male NMRs and compared them to mature adult male mice (6-8 mo, n=4). We first compared the contribution of fatty acids to mitochondrial activity using octanoylcarnitine and malate as substrates. After this, maximum coupled respiration-state (OXPHOS-state) was established by further addition of glutamate and succinate. Finally, we completed the test sequence by adding carbonyl cyanide p-(trifluoromethoxy)-phenylhydrazone (FCCP) in order to achieve the maximum uncoupled respiration-state. We

214 observed (Figure 2E) that NMRs and mice showed similar rates of mitochondrial
215 respiration supported by fatty acids. In contrast, NMR livers show reduced
216 maximum mitochondrial activity compared to mouse liver. In line with the
217 reduced abundance of respiratory chain components, mitochondrial oxygen
218 consumption normalized per wet tissue volume was significantly reduced in
219 both maximum OXPHOS (35% ($p=0.011$) and 37% ($p=0.014$) in 1 and 10 yo
220 NMRs, respectively; one-way ANOVA followed by Bonferroni's t-test), and
221 maximum uncoupled states (51% ($p<0.001$) and 54% ($p<0.001$)). This implies a
222 ~2-fold higher fatty acid supported mitochondrial respiration in NMRs
223 compared to mice (Figure 2F). Taken together, our data indicate a marked
224 rearrangement of energy metabolism in the liver of NMR characterized by an
225 enhanced lipid metabolism and globally reduced level of mitochondrial
226 respiration.
227

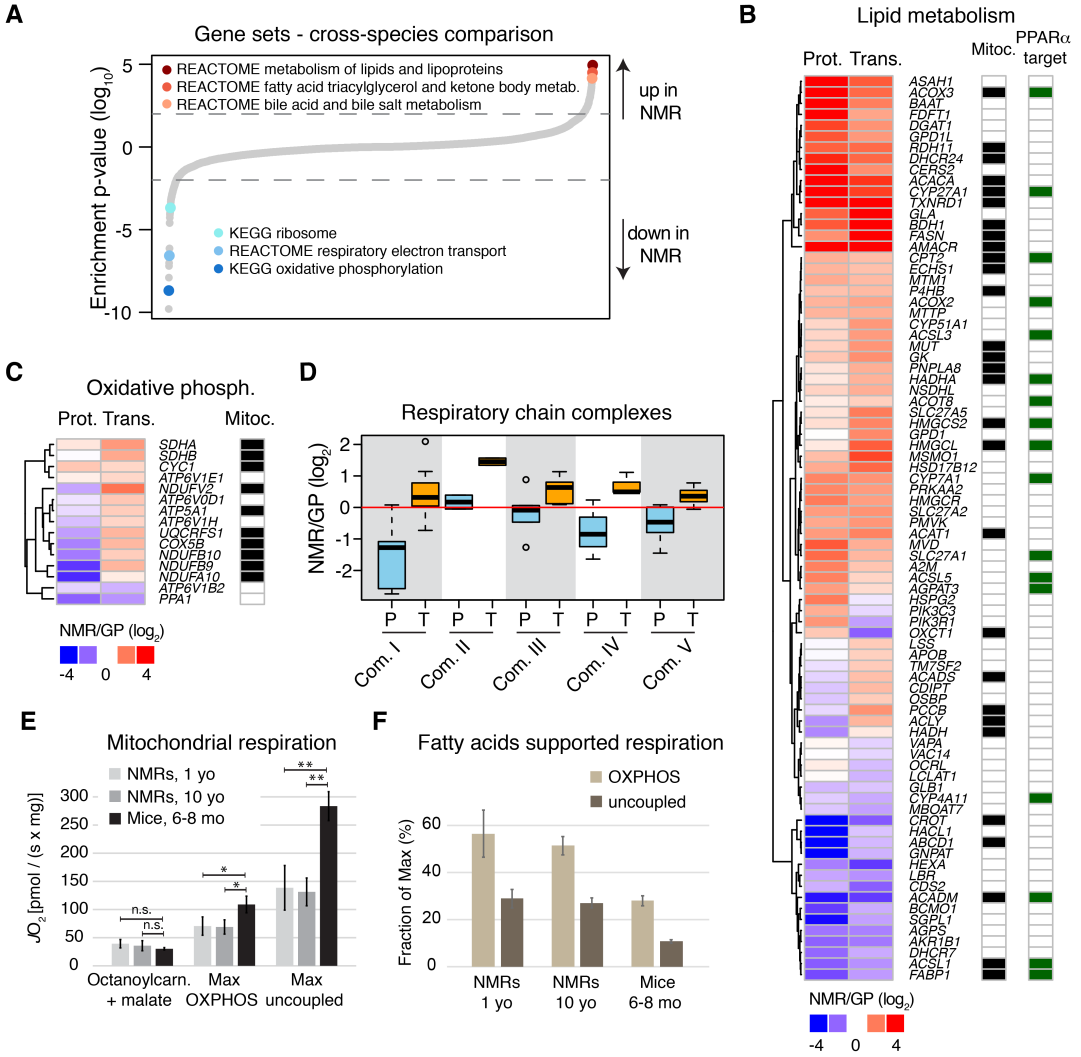

Figure 2. Distinctive features of NMR liver metabolism. (A) Gene set enrichment analysis was performed on proteomic data. Gene sets are plotted according to the $\log_{10}$ value of the calculated enrichment score. Positive and negative values are used for gene sets showing higher and lower abundance in NMR, respectively. Because of the redundancy among the significantly affected gene sets (q<0.05), we highlighted representative categories of gene sets. The complete list of enriched gene sets is available in Table S3. **(B)** Protein (P) and transcript (T) fold changes for genes involved in lipid metabolism ("REACTOME METABOLISM OF LIPIDS AND LIPOPROTEINS", combined RNA-seq and proteome q<0.001), and **(C)** oxidative phosphorylation that are significantly affected in NMR vs. GP (selection criteria as in B). **(D)** Fold changes comparison for genes of the different complexes of the respiratory chain. Light blue and orange boxes indicate protein and transcript fold changes, respectively. **(E)** Mitochondrial oxygen flux supported by octanoylcarnitine and malate, compared to maximum coupled (OXPHOS) and maximum uncoupled respiration in liver of NMR (1 and 10 yo) and 6-8 mo male mice. **(F)** Ratio of fatty acid supported respiration to maximum OXPHOS and uncoupled respiration in liver of NMR and mouse. In E and F, reported values are averages obtained from n=4 animals per experimental group ± standard deviation. *=p<0.05; **=p<0.001; n.s=not significant. Related to Table S3.

250 *Cross-species- and aging-related changes correlate*
251
252 Given the existing evidences linking both lipid metabolism and oxidative
253 phosphorylation to lifespan [30,31], we investigated how these pathways are
254 affected during aging in NMRs. We therefore compared the liver proteome of
255 young (3-4 yo) and old (>20 yo) NMRs using quantitative mass spectrometry
256 (Figure 3A, Table S1 and S4). Gene Ontology analysis, based on 5237 protein
257 groups quantified by at least 2 unique peptides, revealed changes that are typical
258 of the aging process (Figure 3B). These include increased inflammation and
259 immune response-related proteins [23], and accumulation of extracellular
260 matrix proteins [32]. Interestingly, we found a statistically significant overlap
261 between proteins differentially abundant in NMR vs. GP, and proteins whose
262 abundance is affected by NMR aging (99 proteins, $p=2x10^{-4}$, Fisher's exact test,
263 Figure 3C). Additionally, we observed a negative correlation between protein
264 fold changes across species and NMR aging (Pearson R=-0.38, p=0.0001; Figure
265 3D), resulting in a significant difference between cumulative distributions of
266 NMR vs. GP fold changes for proteins up- or down-regulated in NMR aging
267 (p=0.002, Kolmogorov-Smirnov-test; Figure 3E). The directionalities of the
268 differences indicate that proteins with decreasing expression during NMR aging
269 tend to have a higher level in young NMR compared to GP, whereas, proteins
270 with increasing expression during NMR aging tend to start from a lower level in
271 young NMR than in GP. Statistical significance for overlap (p=0.008, Fisher's
272 exact test), anti-correlation of fold changes (Pearson R=-0.18, $p=1.8x10^{-8}$), and
273 difference between cumulative distributions ($p=3.1x10^{-12}$, Kolmogorov-Smirnov-
274 test) can also be observed from RNA-seq data obtained from the same animals
275 (Figure S1). In particular, we found among the 30 liver proteins up in NMR vs. GP
276 and down during NMR aging 13 linked to lipid or fatty acid and 5 to xenobiotic
277 metabolism (Figure 3F). Our data suggest that this group of proteins might be
278 involved in sustaining the longevity of NMRs, and their decline during aging
279 might contribute to a phenotypically/functionally not yet reported reduction of
280 liver function.
281

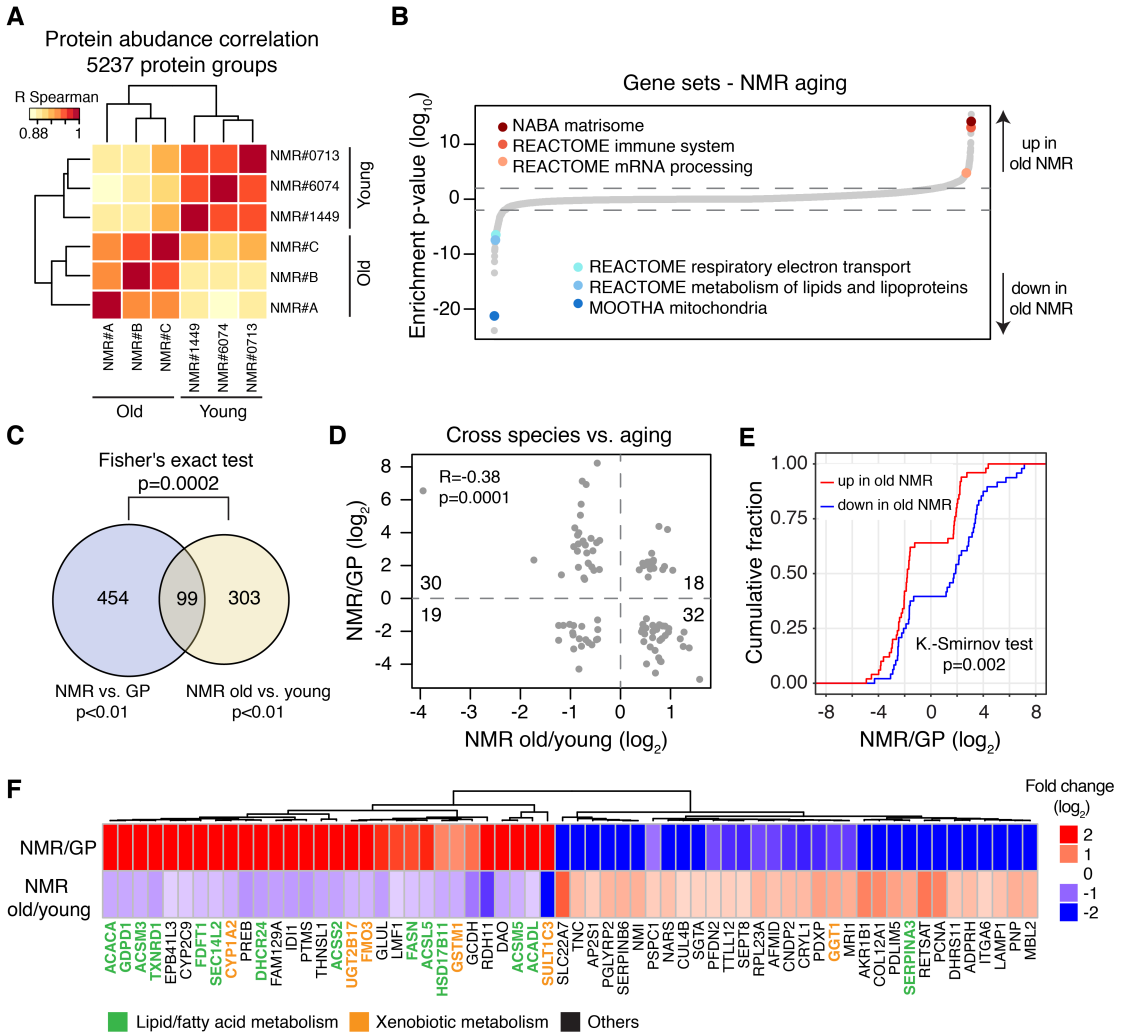

Figure 3. The impact of aging on the NMR liver proteome (A) Livers from 3 young (2.7-3.8 yo) and 3 old (>20 yo) NMRs were compared by Tandem Mass Tags (TMT) based quantitative mass spectrometry. Hierarchical clustering based on the correlation between proteome profiles based on 5237 protein groups cross-quantified between the two age groups (Table S4). **(B)** Gene set enrichment analysis. Gene sets are plotted according to the $\log_{10}$ value of the calculated enrichment score. Positive and negative values are used for gene sets showing higher and lower abundance in old NMRs, respectively. Selected significantly affected gene sets (q<0.05) are highlighted. The complete list of enriched gene sets is available in Table S5. **(C)** Overlap between proteins differentially expressed in NMR vs. GP and affected by aging in NMR. **(D)** Comparison between cross-species and aging-related fold changes for the 99 proteins significantly different in both comparisons. **(E)** Cumulative distributions of significant NMR vs. GP fold differences for the 99 proteins also significantly up- (red) or down- (blue) regulated in aging. **(F)** The 62 proteins with significant but opposite fold changes in both comparisons (Table S6). Proteins involved in lipid/fatty acid metabolism and xenobiotic metabolism are highlighted in green and orange, respectively. Related to Figure S1 and Tables S4, S5 and S6.

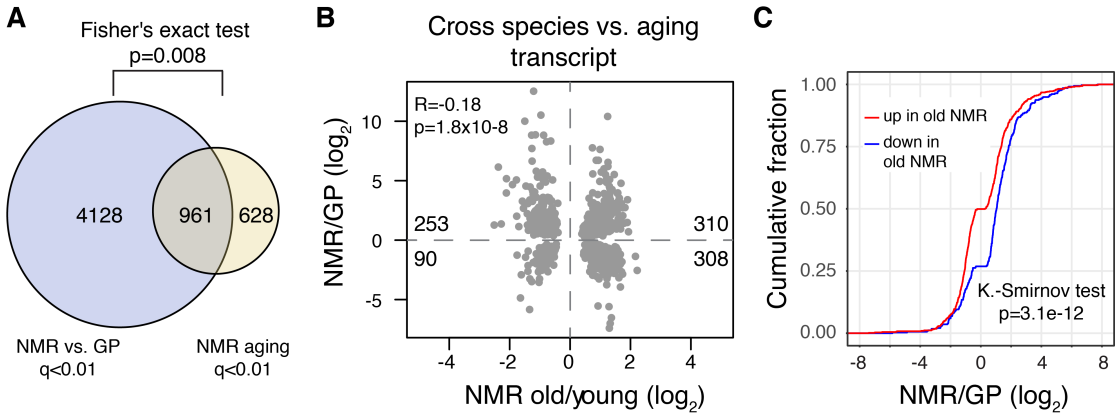

Figure S1. Correlations between liver transcript level differences of NMR vs. GP and during NMR aging. (A) Significant overlap between differentially expressed genes (DEGs) in NMR vs. GP and in aging of NMR. **(B)** Comparison between cross-species and aging-related fold changes for the 875 DEGs significant in both comparison (q<0.01) shows significant negative correlation. **(C)** Cumulative distributions of NMR vs. GP fold changes for the 875 DEGs also significantly up- (red) or down- (blue) regulated in NMR aging. The x-axis was restricted to ±8 for display purpose. Related to Figure 3 and Table S6.

316 *Aging affects similar pathways in both NMR and human liver*
317
318 In order to generalize our findings to other species and in particular to human
319 aging, we analyzed the proteome of donor liver samples from 12 individuals
320 aged between 31 and 88 years (Table S1). In this case, we used formalin fixed
321 and paraffin embedded (FFPE) samples and quantitatively compared the
322 proteomes using mass spectrometry. Principal Component Analysis (PCA) based
323 on 3211 quantified protein groups revealed separation of the proteome profiles
324 based on the age of the donor (Figure 4A). Guided by the PCA analysis, we split
325 the individuals into two groups defined as young (below 50 years of age) and old
326 (above 66 years), and analyzed differential protein expression for 3064 protein
327 groups quantified across all samples (Table S7). Multiple lines of evidence
328 indicate that aging affects similar pathways in both human and NMR liver. First,
329 as in NMR, GO enrichment analysis revealed an age-dependent decline of
330 proteins involved in lipid metabolism and detoxification of xenobiotics, and an
331 increase of proteins related to immune response (Figure 4B and Table S7), and
332 inflammation markers such as RELA/p65 (Figure 4C). Second, enzymes involved
333 in lipid synthesis such as ACACA and DHCR24, which were found to be expressed
334 at higher level in NMR vs. GP and to decline during NMR aging, showed a
335 negative correlation with the age of the donor (Figure 4D and 4E). Enzymes
336 involved in fatty acid beta-oxidation, including ACAA2 and HADHA, also showed
337 a trend of lower abundance in livers from older individuals (Figure S2A). Third,
338 these changes in metabolic enzymes underline a more general reorganization of
339 the liver proteome that is characterized by a significant reduction of both
340 mitochondrial and peroxisomal proteins during aging in both NMR and human
341 (Figure 4F). Fourth, multiple proteins involved in different steps of the
342 xenobiotic metabolism showed similar trends. Cytochrome P450s, a subset of
343 Glutathione S-transferases (GSTs), and UDP-glucuronosyltransferases (UGTs)
344 were in most cases expressed at higher levels in NMR vs. GP and showed an age-
345 dependent decline both in NMR and in human (Figures 4G and S2B). Taken
346 together these data indicate that conserved pathways are affected in NMR and
347 humans during aging.

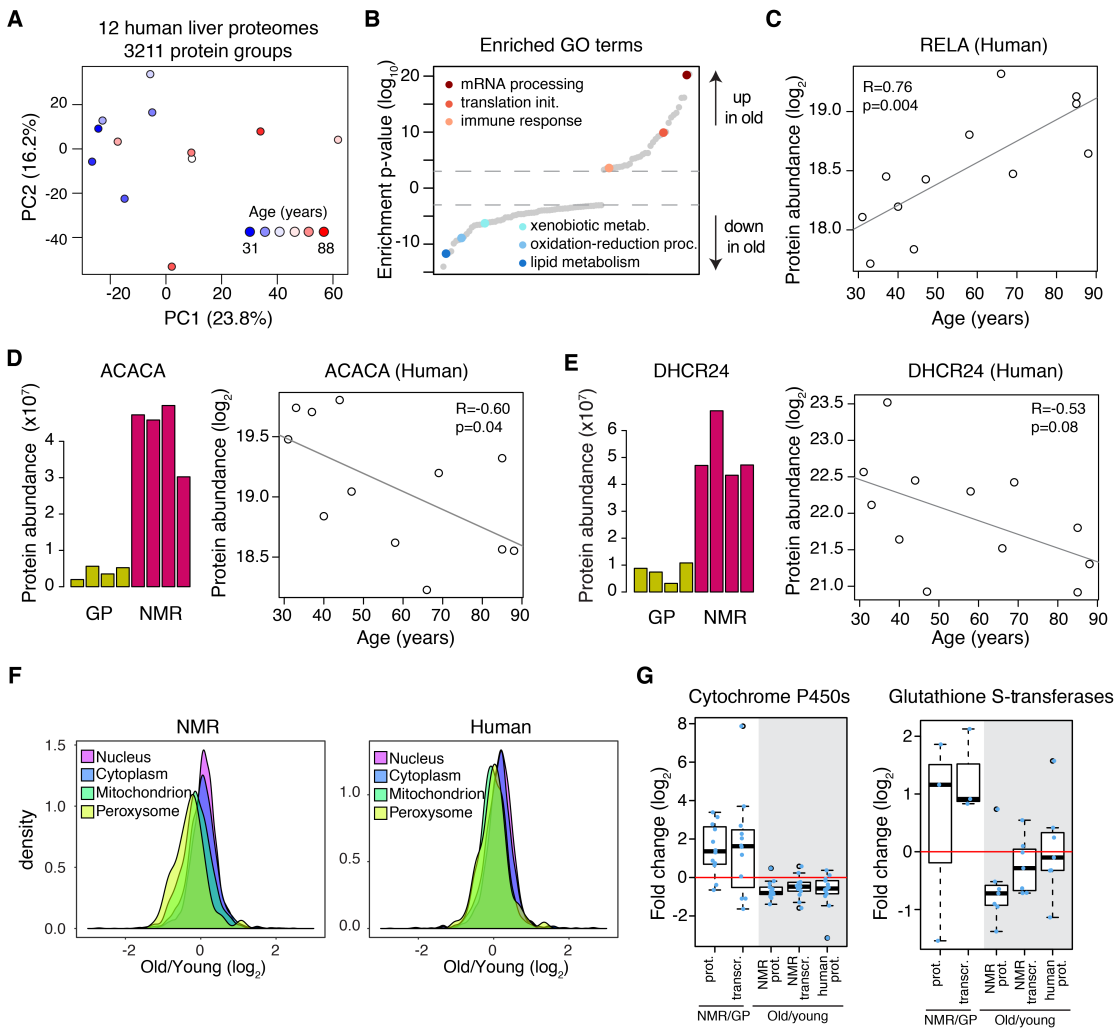

Figure 4. The impact of aging on the human liver proteome and comparison to NMR aging. (A) FFPE liver samples from 12 human donors aged 31-88 years old were analysed by Data Independent Acquisition (DIA) quantitative mass spectrometry. Principal Component Analysis (PCA) of the proteome profiles based on 3211 protein groups quantified. **(B)** Gene Ontology (GO) enrichment analysis based on differential protein expression between young (<47 yo, n=6) and old (>66 yo, n=5) donors. One donor aged 58 yo was excluded from differential expression analysis. GO categories are plotted according to the $\log_{10}$ value of the calculated enrichment p-value. Positive and negative values are used for gene sets showing higher and lower abundance in old individuals, respectively. Selected significantly affected GO terms (p<0.001) are highlighted. The complete list of enriched GO terms is available in Table S7. **(C)** The inflammation marker RELA shows a steady increase of abundance with age. **(D and E)** Selected examples of enzymes involved in lipid metabolism being up regulated in NMR vs. GP and decreasing during aging both in NMRs and humans. **(F)** Mitochondrial and peroxisomal proteins decrease with age in both NMR and human liver. Distributions of fold-changes were calculated separately for proteins assigned to different cellular compartments. Mitochondrial (n=953, $p=1.2\times10^{-37}$ Welch two sample t-test for NMR; n=716, $p=1.4\times10^{-21}$ Welch two sample t-test for human) and peroxisomal proteins (n=95, $p=4.9\times10^{-6}$ Welch two sample t-test for NMR; n= 74, $p=8.9\times10^{-3}$ Welch two sample t-test for human) showed a significant

371 lower abundance in old samples as compared to the rest of the quantified
372 proteins. **(G)** Major categories of detoxifying enzymes differentially expressed in
373 NMR vs. GP and affected by aging in both NMR and humans (only significantly
374 affected cases are shown for each group; cut-offs: NMR vs. GP and NMR aging,
375 combined q<0.05; human proteome aging q<0.1). Related to Figure S2 and Table
376 S7.
377

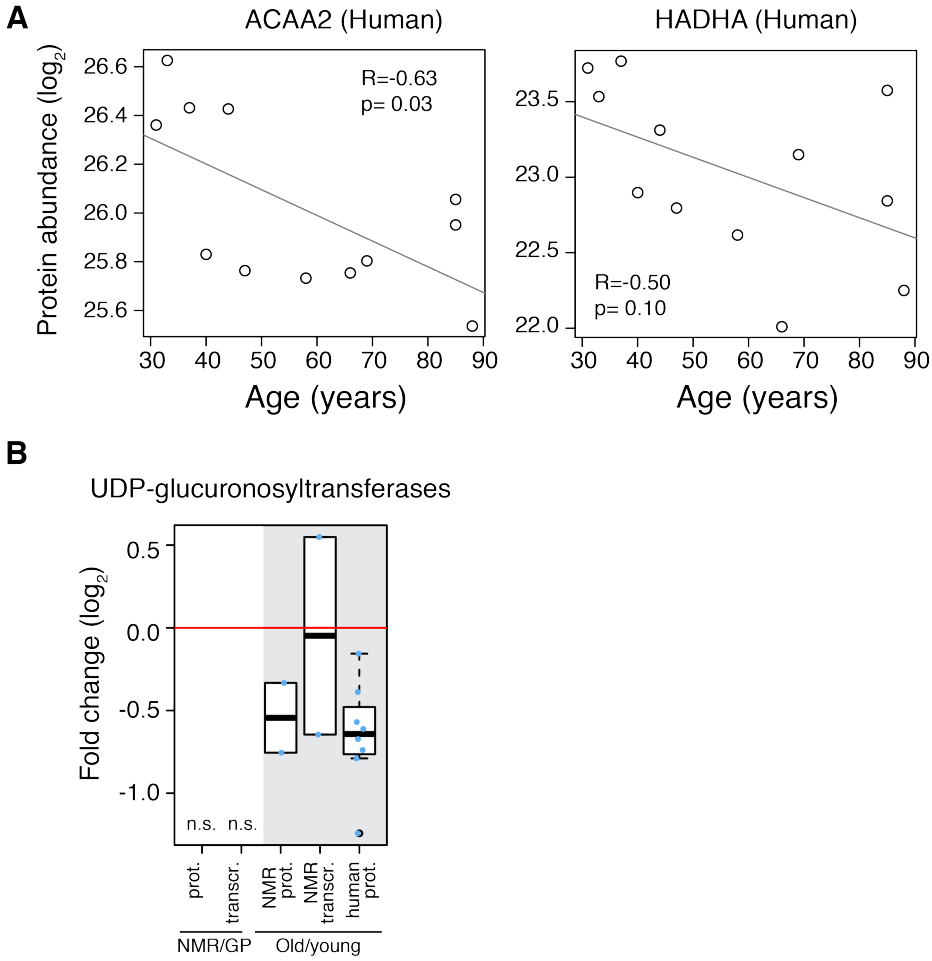

Figure S2. Examples of enzymes involved in fatty acid beta-oxidation and xenobiotic metabolism that decrease during aging in human liver. (A) Additional examples of enzymes involved in lipid metabolism decreasing during aging in human liver. **(B)** Detoxifying enzymes decreasing during aging in both NMR and humans. Only significantly affected genes are shown; cut offs: NMR aging, combined q<0.05; human proteome aging q<0.1; n.s. = no significant cases detected. Related to Figure 4.

390 *The detoxifying enzyme SULT1C3 mediates lifespan extension in C. elegans*
391
392 In order to demonstrate that proteins expressed at higher level in NMR are
393 mechanistically linked to longevity, we focused on proteins involved in
394 xenobiotic metabolism, and in particular the phase II enzyme SULT1C3 and its
395 paralog SULT1C2. These enzymes are expressed at prominent level in NMR and
396 they strongly decline during aging (Figure 5A and Figure S3). The *C. elegans*
397 ortholog of SULTIC2/3 is SSU-1 (coded by *ssu-1*), and it was previously shown to
398 be expressed at high levels in long-lived and stress-resistant dauer larvae
399 (surviving up to 4 months compared to 2-3 weeks lifespan of a reproducing
400 adult). High expression levels of *ssu-1* are thus associated with extended
401 longevity also in worms [33]. The feeding of wild type worms with RNAi against
402 *ssu-1* from L4 larval stage on resulted in significant reduction of their life span
403 (median life span reduction of 13%) suggesting that *ssu-1* is required for normal
404 lifespan of nematodes (Figure 5B). The remarkable stress resistance of dauer
405 larvae is largely due to enhanced expression of pro-survival and detoxification
406 genes mediated by DAF-16/FOXO transcription factor [34,35]. To test whether
407 the FOXO pathway regulates the expression of ssu-1 during adulthood and aging,
408 we performed an epistasis experiment treating *daf-16* deficient nematodes with
409 *ssu-1* RNAi. The lifespan reducing effect of the *ssu-1* RNAi is also observed in *daf-*
410 *16* mutants (median lifespan reduction of 12%) (Figure 5C), suggesting that the
411 function of *ssu-1* in normal aging is regulated by factors other than DAF-
412 16/FOXO.
413

414

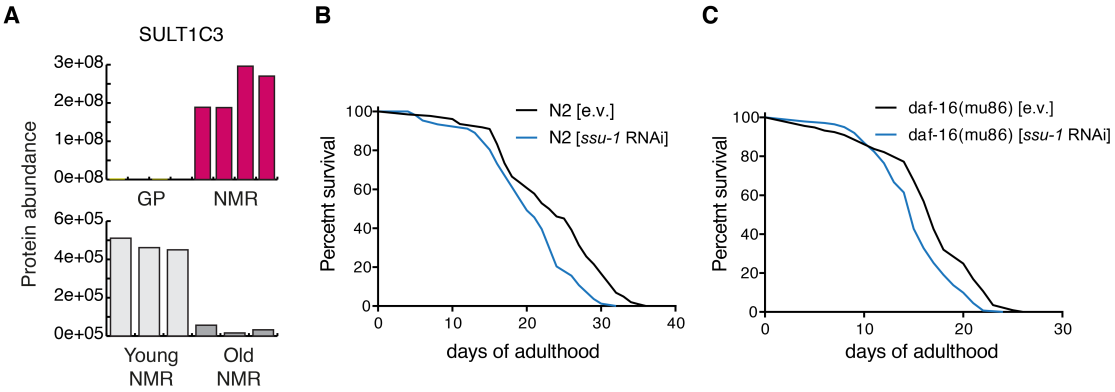

415
416
417 **Figure 5. Knock-down of SSU-1 (*ssu-1)* reduces lifespan in wild type and**
418 ***daf-16(mu86)* mutant *C. elegans*. (A)** The orthologous mammalian phase II
419 conjugation enzyme SULT1C3 is significantly more abundant in NMR compared
420 to GP, and it declines with aging. **(B)** Wildtype (N2, Bristol strain) and **(C)** *daf-*
421 *16(mu86)* mutant worms were treated with *ssu-1* and control empty vector (e.v.)
422 RNAi from the L4 (pre-adult) developmental stage. Survival was scored daily; the
423 significance of lifespan shortening was determined by Mantel-Cox Log rank test
424 ($p<0.0001$ in both cases). Related to Figure S3.
425

426

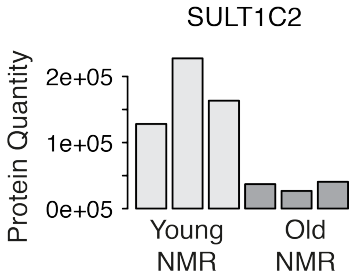

427
428
429 **Figure S3. SULT1C2 decreases with aging in NMR.** Related to Figure 5.
430
431

Discussion:

Cross-species comparisons based on transcriptional profiling have highlighted pathways that correlate with lifespan [1]. In this work, we decided to concentrate on the NMR, as an outlier of exceptional longevity, and directly relate the identified proteome changes to the ones observed in humans, another of those outliers. In our NMR vs. GP comparative approach, we generally observed a good correlation between transcriptome and proteome differences confirming that a great fraction of adaptation to local ecosystems occurs via changes in gene expression that translate into abundance changes of proteins. However, we have identified changes, particularly among complexes of the mitochondrial respiratory chain, which manifested exclusively at the proteome level. Importantly some of these changes are inline with measureable difference in mitochondrial activity in NMR.

Our cross-species analysis revealed that the liver of NMRs possesses three major characteristics compared to GP: (i) lower rate of mitochondrial respiration, due to reduced level of complex I; (ii) higher reliance on fatty acids for energy production, deriving from increased abundance of enzymes responsible for lipid turnover; and (iii) increased expression of detoxifying enzymes. Although we cannot exclude that some of the observed changes derive from differences in diet between the two compared species, the fact that mitochondrial and oxidative phosphorylation genes were identified to be differentially expressed also in NMRs vs. wild mice [7] supports the peculiarity of NMR liver metabolism among rodents. Importantly, we have also shown that the aging process itself negatively affects the abundance of proteins involved in lipid metabolism and detoxification processes both in NMR and humans. These pathways are similarly affected with aging also in mice [36].

Two major questions arise from our work: how NMRs have evolved their particular liver metabolism, and how does this contribute to the extreme longevity of these animals? Multiple studies have previously linked the composition of the mitochondrial respiratory chain to lifespan extension in multiple species [31]: altered composition of the respiratory chain has been show to induce a hormetic response that can extend lifespan in *C.elegans* [37]; mild inhibition of complex I leads to increased lifespan in the short-lived fish *N. furzeri* [38]; low abundance of the matrix arm of complex I predicts longevity in mice [39]; fibroblasts isolated from long lived individuals including centenarians show altered mitochondrial activity with lower complex I driven ATP synthesis [40].

Similarly, lipid homeostasis and signaling has been linked to health and longevity [30], and changes in lipid metabolism have been shown to mediate the positive effects of anti-aging dietary interventions. Dietary interventions such as calorie restriction (CR) or fasting influence lipid metabolism [41,42]. Transcriptomic and metabolomic measurements showed that CR promotes fatty acid fueling of mitochondria in liver of mice and it is accompanied by changes in body fat composition [43]. Both fatty acid oxidation and lipid metabolism pathways as well as xenobiotic metabolism are induced by CR in mouse liver via epigenetic

481 reprogramming [44]. Changes in lipid metabolism are mechanistically linked to
482 activation of stress response pathways that mediate enhanced proteostasis [45],
483 and fatty acid oxidation and functional peroxisomes are required to maintain
484 mitochondria network homeostasis and promote longevity in *C. elegans* [46]. In
485 humans, shifts in body composition accompany aging including a decrease of
486 lean mass and accumulation of body fat. Fatty acid oxidation by respiring tissue
487 decreases with age in humans [47,48], however there are discordant reports
488 [49]. A decrease in fatty acid oxidation during aging can lead to adipose tissue
489 accumulation and thus contribute to increased systemic inflammation, a major
490 risk factor for aging-associated disease such as type II diabetes [50]. Our data
491 show that in both NMR and human liver there is a progressive decline of
492 enzymes responsible for fatty acid turnover. These alterations might contribute
493 to changes in energy metabolism that favor the accumulation of adipose tissue
494 and increased inflammation at older age.
495
496 From a mechanistic point of view, it is conceivable that adaptation to the
497 particular ecosystem of NMRs has selected for characteristics of energy
498 metabolism that in turn enabled extreme longevity via activation of stress
499 pathways (Figure 6). Among these, the NFE2L2 pathway, which control the
500 expression of many of the detoxifying enzymes that we found increased in NMR
501 vs. GP, was shown to have enhanced activity in NMR [11]. The activity of the
502 same pathways tend to decline during aging, as shown here by the decline of
503 their target genes in both NMR and humans, and in different systems [51,52]. It
504 is therefore tempting to speculate that their higher basal activity in the NMR
505 might contribute to its enhanced stress resistance, and ultimately delay the aging
506 process. In line with this hypothesis, genes encoding for both, respiratory
507 electron transport chain and response to oxidative stress have been shown to be
508 under positive selection in the NMR [6]. Additionally, similar molecular networks
509 (lipid metabolism and oxidative stress pathways) are involved in the social
510 status transition from worker to breeder in NMR [53], suggesting common
511 evolutionary constrains and molecular mechanism underlying longevity and
512 eusociality, i.e. reproductive animals' lifelong fecundity coupled with
513 extraordinary life- and healthspan in the NMR [54] and even extended lifespan in
514 other mole-rats [55,56] and longevity. Further work is required to elucidate in
515 detail which aspects of liver metabolism are sufficient to promote lifespan, and
516 what is the molecular basis mediating positive systemic effects that support
517 organism health by delaying aging in NMR.
518

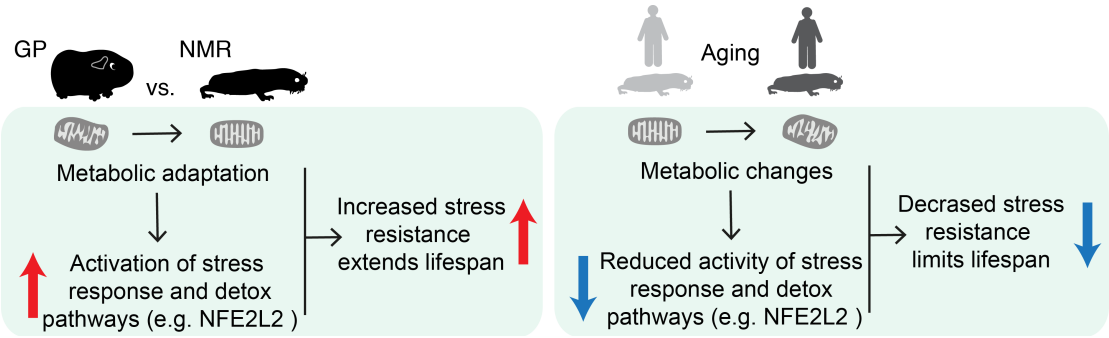

Figure 6. Proposed model linking metabolic changes to stress response/detoxifying pathways in NMR and during aging.

525 **Materials and methods:**
526
527 *Samples*
528
529 Young NMR and GP liver tissue samples were obtained at the Leibniz Institute
530 for Zoo and Wildlife Research, IZW (Berlin, Germany). Old NMR liver tissue
531 samples were obtained from the Stockholm Zoo. Sampling and animal
532 procedures were approved by the local ethics committee of the "Landesamt für
533 Gesundheit und Soziales", Berlin, Germany (reference numbers: #ZH 156,
534 G02217/12, and T 0073/15) and were compliant with the national and
535 institutional animal care guidelines. NMRs were kept inside artificial burrow
536 systems, consisting of acrylic glass containers interconnected with tubes. Except
537 during cleaning and management procedures, animals were kept in complete
538 darkness and supplied daily *ad libitum* with fresh vegetables. Temperature and
539 humidity were kept stable at 27.0±2.0°C and 85.0±5.0%, respectively. GPs
540 (breed: Dunkin Hartley HsdDhl:DH, Harlan Laboratories, AN Venray,
541 Netherlands) were kept pairwise in standardized GP cages with a 12h light-dark
542 cycle. They were fed commercial pellets and fresh vegetables daily; hay and
543 vitamin C enriched water were provided *ad libitum*. Temperature and humidity
544 ranged between 18.0±2.0°C and 45.0±5.0%, respectively. For tissue collection,
545 animals were euthanized by surgical decapitation under general anaesthesia
546 (Isofluran CP, CP-Pharma, Burgdorf, Germany). Tissue samples were fresh frozen
547 and stored in liquid nitrogen before transcriptome or proteome analysis.
548
549 Human liver tissue samples were provided by the tissue bank of the National
550 Center for Tumor Diseases (NCT, Heidelberg, Germany) in accordance with the
551 regulations of the tissue bank and the approval of the ethics committee of
552 Heidelberg University. These samples were obtained in a transplant setting to
553 check the quality of the donor liver by histology before implantation. The age of
554 the donors ranges from 31-88. The tissue samples were formalin fixed, paraffin-
555 embedded (FFPE) and slides were stained with hematoxylin and eosin (H&E).
556 These full-section H&E slides were re-evaluated by a trained pathologist (SS)
557 confirming that each of the samples used for proteomic analyses did not show
558 any overt pathomorphological changes (e.g. necrosis or significant inflammatory
559 or fatty changes).
560
561 *RNA sequencing analysis.*
562
563 <u>Reference transcripts</u>
564 Reference transcripts for NMR are based on recently published de novo
565 transcriptome assembly [57]. Reference transcripts for GP were obtained by *de*
566 *novo* transcriptome assembly of ten different tissue samples as described in [53],
567 using the human transcriptome as a reference for gene symbol assignment. Both
568 transcript sets were mapped to the corresponding genomes (NMR UCSC hetgla2,
569 GP UCSC cavpor3) in two steps: BLAT was used to identify the locus and then
570 SPLIGN (v1.39.8) was applied to splice align the transcript sequence within BLAT
571 locus.
572
573

574 Transcript quantification
575 For NMR age comparison RNA-seq data were aligned to the reference genome
576 utilizing STAR (v2.4.1d) with a maximum mismatch of 6% and a minimum
577 aligned length of 90%. Reads mapped to multiple loci were discarded. Gene
578 expression was quantified using HTSEQ (v0.6.1p1) based on the aligned
579 reference transcripts. For cross-species comparison (NMR vs. GP) orthologous
580 transcribed regions were determined using PosiGene [58] with parameter
581 'prank=0 max_anchor_gaps_hard=100 rs=NMR'. RNA-seq data were aligned to
582 corresponding orthologous transcribed regions in NMR and GP reference
583 transcripts using bowtie2 (2.2.9) with the parameter '--very-sensitive-local'.
584 DESeq2 (v1.6.3) was used to identify DEGs after correction of p-values using
585 Benjamini Hochberg (FDR, denoted as 'q') for NMR aging and cross-species
586 comparison.
587
588 Data availability
589 RNA-seq data of GP used in *de novo* assembly were deposited at Sequence Read
590 Archive (SRP104222). RNA-seq data for NMR age and cross-species comparisons
591 were deposited in Gene Expression Omnibus (GSE98744, GSE98744). The
592 corresponding gene annotation for NMR and GP are available as a gff3-file
593 (ftp://genome.leibniz-fli.de/pub/nmr2017/).
594
595 *Sample preparation for mass spectrometry*
596
597 NMR and GP fresh frozen liver samples for label free cross species comparison
598 Frozen tissue samples of NMR and GP livers (between 20 and 40 mg, Table S1)
599 were collected into Precellys Lysing kit tubes (Keramik-kit 1.4/2.8 mm, 2 mL
600 (CKM)) containing 200 µL of protein solubilization buffer (80 µM Tris pH 8.0, 80
601 µM DTT and 4% SDS) and processed directly. Samples were homogenized in the
602 Precellys 24 homogenizer (Bertin Instruments, France) at 5000 rpm for 30
603 seconds at 4 °C. Samples were then spun down and the supernatant transferred
604 to a 1.5 mL Eppendorf tube. Samples were sonicated using a Bioruptor Plus
605 (Diagenode) for 7.5 minutes (5 cycles: 1 min on, 30 sec off, 20 °C) using the high
606 setting, and then boiled for 10 min at 95°C. A second round of sonication (as
607 before) followed the boiling. Samples were spun down at 20800x *g* for 5 minutes
608 and the lysate supernatant transferred to fresh tubes. Protein concentration was
609 determined by BCA assay (Pierce) using standard protocol and adjusted to 10
610 µg/µL using solubilization buffer. 5 µL of tissue lysate, corresponding to 50 µg
611 protein, was taken for preparation for MS. Cysteine residues were alkylated by
612 adding 1 µL of, 200 mM iodoacetamide to a final concentration of 15 mM
613 (incubated for 30 min at room temperature in the dark). Reaction was quenched
614 by addition of 1 µL of 200 mM DTT. Sample clean-up proceeded following a
615 modified SP3 protocol. Sera-Mag Speed Beads (#45152105050250 and
616 #65152105050250, Thermo Scientific) were mixed 1:1, rinsed with water and
617 stored as a 40 µg/µL stock solution in 4°C, as described in [59]. 4 µL of beads
618 stock was added to the reaction tube and mixed by pipetting then 11 µL
619 acetonitrile containing 5% (v/v) formic acid was added. Samples were incubated
620 for 8 minutes at room temperature to allow protein bindings to the beads. Next,
621 tubes were placed on the magnetic rack. Supernatant was removed and
622 discarded. Beads were washed twice with 180 µL of 70% (v/v) ethanol and once

623 with 180 µL of 100% acetonitrile. After removal of acetonitrile beads were air-
624 dried for 60 sec and then resuspended in 7 µL of digestion buffer (6 µL 4 M urea
625 in 100 mM ammonium bicarbonate and 1 µL of 1 µg/µL of LysC (Wako)).
626 Samples were sonicated for 5 min in water bath, incubated for 5 min at 37°C and
627 then mixed by pipetting. Digestion was allowed to proceed for 4 h at 37°C. After
628 the first step of digestion, beads were resuspended by pipetting, urea was diluted
629 to the final concentration of 1.5 M and 1 µL of 1 µg/µL of sequencing grade
630 trypsin (Promega) was added to samples. Digestion was performed overnight at
631 37°C. After digestion, beads were resuspended by pipetting. 100% acetonitrile
632 was added to the final concentration of 95% (v/v) and samples were incubated
633 for 8 min at room temperature. Tubes were placed on the magnetic rack and
634 washed twice with 100% acetonitrile. Supernatant was removed and beads air-
635 dried and reconstituted in 20 µL of 2% DMSO followed by 5 min of sonication in
636 the water bath. Samples were resuspended by pipetting and placed on the
637 magnetic rack. Supernatant containing peptides was transferred to a fresh tube
638 and acidified with 2 µL of 1% (v/v) formic acid prior to pre-fractionation by high
639 pH reverse phase chromatography. Offline high pH reverse phase fractionation
640 was performed using an Agilent 1260 Infinity HPLC System equipped with a
641 binary pump, degasser, variable wavelength UV detector (set to 220 and 254
642 nm), peltier-cooled autosampler (set at 10°C) and a fraction collector. The
643 column was a Waters XBridge C18 column (3.5 µm, 100 x 1.0 mm, Waters) with a
644 Gemini C18, 4 x 2.0 mm SecurityGuard (Phenomenex) cartridge as a guard
645 column. The solvent system consisted of 20 mM ammonium formate (pH 10.0) as
646 mobile phase (A) and 100% acetonitrile as mobile phase (B). The separation was
647 accomplished at a mobile phase flow rate of 0.1 mL/min using a linear gradient
648 from 100% A to 35 % B in 61 min. Thirty-four fractions were collected along
649 with the LC separation, which were subsequently pooled into 10 fractions.
650 Pooled fractions were dried in a Speed-Vac and then stored at -80°C until LC-
651 MS/MS analysis.
652
653 <u>NMR frozen liver samples for TMT-based comparison of young and old samples</u>
654 For each experimental animal (Table S1), 100 µg protein lysate from the bead-
655 beaten stock of tissue described above were taken up to a final volume of 50 µL
656 with 100 mM HEPES buffer, pH 8.5. 5 µL of 2% SDS was added, prior to
657 biorupting (5 cycles: 1 min on, 30 sec off, 20 °C) at the highest settings. Samples
658 were spun down at 20800x *g* for 1 minute and the lysate supernatant transferred
659 to fresh tubes. Reduction was performed with 2.9 µL DTT (200 mM) for 15
660 minutes at 45 °C before alkylation with 200 mM IAA (5 µL, 30 minutes, room
661 temperature, in the dark). Proteins were then precipitated with 4 volumes ice
662 cold acetone to 1 volume sample and left overnight at -20 °C. The samples were
663 then centrifuged at 20800x *g* for 30 minutes, 4 °C. After removal of the
664 supernatant, the precipitates were washed twice with 500 µL 80% (v/v) acetone
665 (ice cold). After each wash step, the samples were vortexed, then centrifuged
666 again for 2 minutes at 4°C. The pellets were then allowed to air-dry before being
667 dissolved in digestion buffer (50 µL, 3M urea in 0,1M HEPES, pH 8; 1 µg LysC)
668 and incubated for 4 h at 37 °C with shaking at 600 rpm. Then the samples were
669 diluted 1:1 with milliQ water (to reach 1.5M urea) and were incubated with 1 µg
670 trypsin for 16 h at 37 °C. The digests were then acidified with 10% trifluoroacetic
671 acid and then desalted with Waters Oasis® HLB µElution Plate 30µm in the

672 presence of a slow vacuum. In this process, the columns were conditioned with
673 3x100 µL solvent B (80% (v/v) acetonitrile; 0.05% (v/v) formic acid) and
674 equilibrated with 3x 100 µL solvent A (0.05% (v/v) formic acid in milliQ water).
675 The samples were loaded, washed 3 times with 100 µL solvent A, and then eluted
676 into PCR tubes with 50 µL solvent B. The eluates were dried down with the speed
677 vacuum centrifuge and dissolved in 200 mM HEPES buffer, pH 8.5 for TMT
678 labeling. 25 µg peptides were taken for each labeling reaction at 1 µg/µL
679 concentration. TMT-6plex reagents (Thermo Scientific) were reconstituted in 41
680 µL 100% anhydrous DMSO. TMT labeling was performed by addition of 2.5 µL of
681 the TMT reagent. After 30 minutes of incubation at room temperature, with
682 shaking at 600 rpm in a thermomixer (Eppendorf) a second portion of TMT
683 reagent (2.5 µL) was added and incubated for another 30 minutes. The reaction
684 was quenched with 1 µL of 20 mM lysine in 100 mM ammonium bicarbonate.
685 After checking labeling efficiency, samples were pooled (48 µg total), cleaned
686 once again with Oasis and subjected to high pH fractionation prior to MS
687 analysis. Offline high pH reverse phase fractionation was performed as described
688 above with the following modifications for TMT labeled samples: (i) the
689 separation was accomplished at a mobile phase flow rate of 0.1 mL/min using a
690 non-linear gradient from 95% A to 40 % B in 91 min; (ii) 48 fractions were
691 collected along with the LC separation that were subsequently pooled into 16
692 fractions.
693
694 <u>Human FFPE liver samples</u>
695 The specimens were cut on a microtome into 5 µm thick sections and mounted
696 on glass slides. Slides were deparaffinized in xylene for 2x 5 minutes, rehydrated
697 in 100% ethanol for 2x 5 minutes, and then washed in 96% (v/v), 70% (v/v),
698 50% (v/v) ethanol and milliQ water for 1x 5 minutes each. Region of interest
699 were gently scraped using a scalpel and transferred to a PCR tube containing 100
700 µL of protein solubilization buffer (80 µM Tris pH 8.0, 80 µM DTT and 4% SDS)
701 and processed directly. Samples were sonicated using a Bioruptor Plus
702 (Diagenode) for 25.2 min (15 cycles: 1 min on, 30 sec off) at 20°C using the high
703 setting, and then boiled for 1h at 99°C. Sonication followed by boiling was
704 performed twice. Cysteine residues were alkylated by adding 200 mM
705 iodoacetamide to a final concentration of 15 mM (incubated for 30 min at room
706 temperature in the dark). Reaction was quenched by addition of 10 µL of 200
707 mM DTT. Protein were then acetone precipitated, digested and desalted as
708 described above for NMR samples (aging comparison), with the exceptions that
709 0.5 µg of both LysC and trypsin were used instead of 1 µg to accommodate for the
710 lower amount of protein extract employed, and no TMT labeling was performed.
711
712 *Mass spectrometry data acquisition*
713
714 <u>Label free analysis of NMR and GP liver samples</u>
715 For label free experiments, each fraction from the 4 GP and 4 NMR samples,
716 separated by high pH, were resuspended in 10 µL reconstitution buffer (5%
717 (v/v) acetonitrile, 0.1% (v/v) TFA in water) and 8 µL were injected. Peptides
718 were separated using the nanoAcquity UPLC system (Waters) fitted with a
719 trapping (nanoAcquity Symmetry C18, 5 µm, 180 µm x 20 mm) and an analytical
720 column (nanoAcquity BEH C18, 2.5 µm, 75 µm x 250 mm). The outlet of the

721 analytical column was coupled directly to an Orbitrap Fusion Lumos (Thermo
722 Fisher Scientific) using the Proxeon nanospray source. Solvent A was water,
723 0.1% (v/v) formic acid and solvent B was acetonitrile, 0.1% (v/v) formic acid.
724 The samples were loaded with a constant flow of solvent A at 5 µL/min, onto the
725 trapping column. Trapping time was 6 min. Peptides were eluted via the
726 analytical column at a constant flow of 0.3 µL/min, at 40°C. During the elution
727 step, the percentage of solvent B increased in a linear fashion from 5% to 7% in
728 10 minutes, then from 7% B to 30% B in a further 105 min and to 45% B by 130
729 min. The peptides were introduced into the mass spectrometer via a Pico-Tip
730 Emitter 360 µm OD x 20 µm ID; 10 µm tip (New Objective) and a spray voltage of
731 2.2kV was applied. The capillary temperature was set at 300°C. Full scan MS
732 spectra with mass range 375-1500 *m/z* were acquired in profile mode in the
733 Orbitrap with resolution of 120000 using the quad isolation. A first batch of
734 samples (NMR: F1-6074, M1-1449; GP: #18, #19) was acquired with the
735 following settings. The RF on the ion funnel was set to 60%. The filling time was
736 set at maximum of 100 ms with an AGC target of 4 x 10^5 ions and 1 microscan.
737 The peptide monoisotopic precursor selection was enabled along with relaxed
738 restrictions if too few precursors were found. The most intense ions (instrument
739 operated for a 3 second cycle time) from the full scan MS were selected for MS2,
740 using quadrupole isolation and a window of 1.6 Da. An intensity threshold of 5
741 x10^3 ions was applied. HCD was performed with collision energy of 35%. A
742 maximum fill time of 30 ms with an AGC target of 1 x 10^4 for each precursor ion
743 was set. MS2 data were acquired in centroid in the ion trap, in Rapid scan mode,
744 with fixed first mass of 120 *m/z*. The dynamic exclusion list was with a maximum
745 retention period of 60 sec and relative mass window of 10 ppm. In order to
746 improve the mass accuracy, internal lock mass correction using a background ion
747 (*m/z* 445.12003) was applied. For data acquisition and processing of the raw
748 data Xcalibur 4.0 (Thermo Scientific) and Tune version 2.0 were employed. As a
749 consequence of method optimization, the following parameters were changed
750 for a second batch of samples (NMR: #0713, #4925; GP: #23, #28): RF on the ion
751 funnel was set to 40%, AGC target to 2 x 10^5, quadrupole isolation window to 1.4
752 Da, HCD collision energy to 30%, fill time to 300 ms, AGC target to 2 x 10^3, and
753 the instrument was set to inject ions for all available parallelizable time. Since
754 the two batches of samples were block randomized (i.e. both contained the same
755 number of NMR and GP samples), the usage of two different methods did not
756 influence the outcome of our comparison, as shown by the expected clustering of
757 the samples according to the species of origin (Figure 1B).
758
759 <u>TMT analysis of NMR young and old samples</u>
760 For TMT-6plex experiments, fractions were resuspended in 10 µL reconstitution
761 buffer (5% (v/v) acetonitrile, 0.1% (v/v) TFA in water) and 3.5 µL were injected.
762 Peptides were analyzed using the same LC-MS/MS setup described above with
763 the following modifications. Peptides were eluted using a linear gradient from
764 5% to 7% in 10 minutes, then from 7% B to 30% B in a further 105 min and to
765 45% B by 130 min. Full scan MS spectra with mass range 375-1500 *m/z* were
766 acquired in profile mode in the Orbitrap with resolution of 60000 using the quad
767 isolation. The RF on the ion funnel was set to 40%. The filling time was set at
768 maximum of 100 ms with an AGC target of 4 x 10^5 ions and 1 microscan. The
769 peptide monoisotopic precursor selection was enabled along with relaxed

770 restrictions if too few precursors were found. The most intense ions (instrument
771 operated for a 3 second cycle time) from the full scan MS were selected for MS2,
772 using quadrupole isolation and a window of 1 Da. HCD was performed with
773 collision energy of 35%. A maximum fill time of 50 ms for each precursor ion was
774 set. MS2 data were acquired with fixed first mass of 120 *m/z*. The dynamic
775 exclusion list was with a maximum retention period of 60 sec and relative mass
776 window of 10 ppm. For the MS3, the precursor selection window was set to the
777 range 400-2000 m/z, with an exclude width of 18 *m/z* (high) and 5 *m/z* (low).
778 The most intense fragments from the MS2 experiment were co-isolated (using
779 Synchronus Precursor Selection = 8) and fragmented using HCD (65%). MS3
780 spectra were acquired in the Orbitrap over the mass range 100-1000 *m/z* and
781 resolution set to 30000. The maximum injection time was set to 105 ms and the
782 instrument was set not to inject ions for all available parallelizable time.
783
784 Data Independent Acquisition (DIA) for human FFPE samples
785 Peptides were spiked with retention time HRM kit (Biognosys AG), and analyzed
786 using the same LC-MS/MS setup described above with the following
787 modifications. Approx. 1 µg for Data Dependent Acquisition (DDA) and 3 µg for
788 DIA analysis were loaded. Peptides were eluted via a non-linear gradient from 0
789 % to 40 % in 120 minutes. Total runtime was 145 minutes, including clean-up
790 and column re-equilibration. The RF lens was set to 30%. For spectral library
791 generation, a pooled sample was generated by mixing equal portion of each
792 sample, injected 12 times, and measured in DDA mode. The conditions for DDA
793 data acquisition were as follows: Full scan MS spectra with mass range 350-
794 1650 *m/z* were acquired in profile mode in the Orbitrap with resolution of
795 60000. The filling time was set at maximum of 50 ms with limitation of 2 x 10^5
796 ions. The "Top Speed" method was employed to take the maximum number of
797 precursor ions (with an intensity threshold of 5 x 10^4) from the full scan MS for
798 fragmentation (using HCD collision energy, 30%) and quadrupole isolation (1.4
799 Da window) and measurement in the Orbitrap (resolution 15000, fixed first
800 mass 120 *m/z*), with a cycle time of 3 seconds. The MIPS (monoisotopic
801 precursor selection) peptide algorithm was employed but with relaxed
802 restrictions when too few precursors meeting the criteria were found. The
803 fragmentation was performed after accumulation of 2 x 10^5ions or after filling
804 time of 22 ms for each precursor ion (whichever occurred first). MS/MS data
805 were acquired in centroid mode. Only multiply charged (2^+ - 7^+) precursor ions
806 were selected for MS/MS. Dynamic exclusion was employed with maximum
807 retention period of 15s and relative mass window of 10 ppm. Isotopes were
808 excluded. For data acquisition and processing Tune version 2.1 was employed.
809 For the DIA data acquisition the same gradient conditions were applied to the LC
810 as for the DDA and the MS conditions were varied as follows: Full scan MS
811 spectra with mass range 350-1650 *m/z* were acquired in profile mode in the
812 Orbitrap with resolution of 120000. The filling time was set at maximum of 20
813 ms with limitation of 5 x 10^5 ions. DIA scans were acquired with 34 mass
814 window segments of differing widths across the MS1 mass range with a cycle
815 time of 3 seconds. HCD fragmentation (30% collision energy) was applied and
816 MS/MS spectra were acquired in the Orbitrap with a resolution of 30000 over
817 the mass range 200-2000 *m/z* after accumulation of 2 x 10^5 ions or after filling

818 time of 70 ms (whichever occurred first). Ions were injected for all available
819 parallelizable time. Data were acquired in profile mode.
820
821 *Mass spectrometry data analysis*
822
823 Label free cross-species comparison of NMR and GP liver samples
824 The Andromeda search engine [60], part of MaxQuant (version 1.5.3.28) [61] was
825 used to search the data. The data for GP and NMR were searched separately
826 against translated species-specific reference transcripts (see RNA sequencing
827 analysis). Database with a list of common contaminants were appended in both
828 cases. The data were searched with the following modifications:
829 Carbamidomethyl (C) (Fixed), and Oxidation (M) and Acetyl (Protein N-term)
830 (Variable). The mass error tolerance for the full scan MS spectra was set at 20
831 ppm and for the MS/MS spectra at 0.5 Da. A maximum of 2 missed cleavages
832 were allowed. Peptide and protein level 1% FDR were applied using a target-
833 decoy strategy [62]. iBAQ (label free quantification) values from the MaxQuant
834 output were used to perform cross-species differential protein expression
835 analysis using scripts written in R (v3.4.1). After removal of reverse and
836 contaminant hits, only protein groups quantified by at least two unique peptides
837 were retained. Common human gene symbols were used to combine iBAQ values
838 for NMR and GP samples. Only protein groups quantified in at least two animals
839 per group were retained when comparing protein abundances between NMR
840 and GP. To reduce technical variation, data were $\log_2$ transformed and quantile-
841 normalized using the preprocessCore library. Protein differential expression was
842 evaluated using the limma package [63]. Differences in protein abundances were
843 statistically determined using the Student's t test moderated by the empirical
844 Bayes method. P values were adjusted for multiple testing using the Benjamini-
845 Hochberg method [64] (Table S2).
846
847 TMT-based analysis of young and old NMR livers
848 TMT-6plex data were processed using Proteome Discoverer v2.0 (Thermo Fisher
849 Scientific). Data were searched against the NMR fasta database using Mascot
850 v2.5.1 (Matrix Science) with the following settings: Enzyme was set to trypsin,
851 with up to 1 missed cleavage. MS1 mass tolerance was set to 10 ppm and MS2 to
852 0.5 Da. Carbamidomethyl cysteine was set as a fixed modification and oxidation
853 of Methionine as variable. Other modifications included the TMT-6plex
854 modification from the quan method used. The quan method was set for reporter
855 ions quantification with HCD and MS3 (mass tolerance, 20 ppm). The false
856 discovery rate for peptide-spectrum matches (PSMs) was set to 0.01 using
857 Percolator [65]. Reporter ion intensity values for the filtered PSMs were
858 exported and processed using in-house written R scripts to remove common
859 contaminants and decoy hits Additionally only PSMs having reporter ion
860 intensities above 1×10^3 in all the relevant TMT channels were retained for
861 quantitative analysis. Only protein groups quantified by at least two unique
862 peptides were analyzed for differential expression between young and old NMR.
863 Data were analysed using the MSnbase package [66]. Reporter ion intensities
864 were $\log_2$-transformed and normalized using the vsn package [67]. Peptide-level
865 data were summarized into their respective protein groups by taking the median

866 value. Differential protein expression was assessed using the limma package, as
867 described above (Table S4).
868
869 DIA analysis of FFPE human samples
870 For library creation, the DDA data was searched using the Andromeda search
871 engine built in MaxQuant (version 1.5.3.28). The data were searched against a
872 human database (Swiss-Prot entries of the Uniprot KB database release 2016_01,
873 20198 entries) with a list of common contaminants appended, as well as the
874 HRM peptide sequences. The data were searched with the following
875 modifications: Carbamidomethyl (C) (Fixed) and Oxidation (M)/ Acetyl (Protein
876 N-term) (Variable). The mass error tolerance for the full scan MS and MS/MS
877 spectra was set at 20 ppm. A maximum of 1 missed cleavage was allowed. The
878 identifications were filtered to satisfy FDR of 1 % on peptide and protein level. A
879 spectral library was created from the MaxQuant output of the DDA runs
880 combined using Spectronaut (version 10, Biognosys AG). This library contained
881 58296 precursors, corresponding to 4624 protein groups using Spectronaut
882 protein inference. DIA data were then uploaded and searched against this
883 spectral library. Precursor matching, protein inference and quantification was
884 performed in Spectronaut using default settings [68]. Differential protein
885 expression was evaluated using a pairwise t-test performed at the precursor
886 level followed by multiple testing correction according to [69]. The data
887 (candidate table, Table S7) was exported from Spectronaut and used for further
888 data analyses (see below).
889
890 *Data analysis*
891
892 For integrated analysis of RNA-seq and proteomic data, transcripts and protein
893 groups were matched using the corresponding gene symbol, P values were
894 combined using the Fisher method, followed by correction for multiple testing
895 using the Benjamini-Hochberg method [64]. Gene set enrichments (Figures 2A
896 and 3B) were performed with the R package *gage* [70] using gene set definitions
897 from the Molecular Signatures Database (MSigDB, C2 v5.1) [71]. Gene Ontology
898 enrichment analysis (Figure 4B) was performed the list of quantified proteins
899 that were ranked according to the level of differential expression (fold change)
900 using GOrilla (Eden et al., 2009) followed by GO term redundancy reduction
901 performed by REViGO [72] using default settings.
902
903 *Measurements of mitochondrial activity*
904
905 Mitochondrial respiration was measured in homogenized liver tissue samples of
906 NMRs and mice by means of high-resolution respirometry using the Oroboros®
907 Oxygraph-2K (Oroboros Instruments, Innsbruck, Austria). This device allows for
908 simultaneous recording the O_2 concentration in two parallel chambers calibrated
909 for 2 ml of respiration medium containing 110 mM D-Sucrose (Sigma 84097), 60
910 mM K-lactobionate (Aldrich 153516), 0.5 mM ethylene glycol tetra acetic acid
911 (Sigma E4378), 1 g/L bovine serum albumin free from essentially fatty acids
912 (Sigma A 6003), 3 mM $MgCl_2$ (Scharlau MA0036), 20 mM taurine (Sigma T0625),
913 10 mM KH_2PO_4 (Merck 104873), 20mM HEPES (Sigma H7523), adjusted to pH
914 7.1 with KOH and equilibrated with 21% O_2 at 37°C. Mitochondrial respiration

915 was quantified in terms of oxygen flux (JO_2) calculated as the rate of change of
916 the O_2 concentration in the chambers normalized for wet tissue volume.
917 The liver tissue homogenates were generated from 40-50 mg of wet tissue
918 samples suspended in 2 ml of ice-cold respiration medium. Aliquots of the
919 homogenates were added to each oxygraph chamber in order to obtain a final
920 amount of 4 mg of NMR liver tissue or 2 mg of mouse liver tissue per chamber.
921 The different amount of tissue was chosen in order to obtain similar absolute
922 *J*O2-values, i.e. *J*O2-values not normalized per wet weight, in both species. Every
923 sample was measured in duplicates; the mean values from both chambers were
924 used for statistical analysis.
925 The titration sequence used for the experiments was as follows: 2 mM malate + 1
926 mM octanoylcarnitine, 5 mM ADP, 10 µM cytochrome c, 10 mM glutamate, 10
927 mM succinate, 2.5 µM oligomycin, 1 µM carbonyl cyanide p-(trifluoromethoxy)-
928 phenylhydrazone (FCCP), 0.5 µM rotenone, and 5 µM antimycin A. The JO_2-values
929 after addition of octanoyl carnitine, malate, ADP, and cytochrome c allow
930 quantifying fatty acid oxidation. The addition of cytochrome c after ADP is
931 required to test the integrity of the outer mitochondrial membrane. If
932 homogenization steps damaged the mitochondrial membrane, addition of
933 cytochrome c induces an increase of the respiratory values. The maximum
934 oxidative capacity of the mitochondrial respiratory chain in the coupled state
935 (maximum OxPhos) was then determined after the subsequent addition of
936 glutamate and succinate. Further injections of the ATP synthase inhibitor
937 oligomycin and of the uncoupler FCCP allowed obtaining the maximum
938 respiratory activity in the uncoupled state. In the next two steps, complex I and
939 complex III were sequentially inhibited by administration of rotenone and
940 antimycin A respectively. Finally sequentially injecting 2 mM ascorbate and 0.5
941 mM of the complex IV substrate tetramethyl phenylene diamine (TMPD) in the
942 parallel chambers allowed for selectively quantifying the activity of the
943 cytochrome-c-oxidase (COX). Part of the JO_2 induced by the injection of TMPD is
944 caused by auto-oxidation of this compound. Therefore, inhibiting the COX by 40
945 µM sodium sulfide allowed to quantify and thus to subtract this auto-oxidation
946 related part from the total JO_2 value under TMPD.
947
948 *C.elegans lifespan measurements*
949
950 HT115 bacteria containing specific RNAi constructs were grown on lysogeny
951 broth agar plates supplemented with ampicillin and tetracycline. Plates were
952 kept at 4°C. Overnight cultures were grown in lysogeny broth media containing
953 ampicillin. RNAi expression was induced by adding 1 mM
954 isopropylthiogalactoside (IPTG) and incubating the cultures at 37°C for
955 20 minutes before seeding bacteria on NGM agar supplemented with ampicillin
956 and 3 mM IPTG. Synchronized L4 larvae were placed on 60 mm dishes containing
957 RNAi expressing bacteria at a density of 70 worms per plate. Worms were
958 transferred to new plates on a daily basis until adulthood day 6 (AD6) and later
959 transferred to new plates every 3-4 days. The number of dead animals was
960 scored daily. The analysis of the lifespan data including statistics was performed
961 using GraphPad Prism software.
962

Acknowledgements:

We thank Stefan Pietsch for support with bioinformatics analysis. We gratefully acknowledge support from the FLI proteomics, sequencing, and bioinformatics core facilities. The FLI is a member of the Leibniz Association and is financially supported by the Federal Government of Germany and the State of Thuringia. We thank Veronika Geißler and other members of NCT tissue bank for their support.

Author contributions:

IH, EC, SH, MV performed experiments and analysed data; MB, AS, KS, NR analysed data; MP, TH, AO, SS, JMK, KS, EC, ME designed experiments; MP, TH and AO oversaw the project and wrote the manuscript.

977 **References:**
978

979 1. Fushan AA, Turanov AA, Lee S-G, Kim EB, Lobanov A V, Yim SH, et al. Gene
980 expression defines natural changes in mammalian lifespan. Aging Cell. 2015;14:
981 352–65. doi:10.1111/acel.12283

982 2. Sahm A, Bens M, Szafranski K, Holtze S, Groth M, Goerlach M, et al. Long-lived
983 rodents reveal signatures of positive selection in genes associated with lifespan
984 and eusociality. doi.org. Cold Spring Harbor Laboratory; 2017; 191999.
985 doi:10.1101/191999

986 3. Lewis KN, Mele J, Hornsby PJ, Buffenstein R. Stress resistance in the naked mole-
987 rat: the bare essentials - a mini-review. Gerontology. Karger Publishers; 2012;58:
988 453–62. doi:10.1159/000335966

989 4. Skulachev VP, Holtze S, Vyssokikh MY, Bakeeva LE, Skulachev M V., Markov A V.,
990 et al. Neoteny, Prolongation of Youth: From Naked Mole Rats to "Naked Apes"
991 (Humans). Physiol Rev. 2017;97: 699–720. doi:10.1152/physrev.00040.2015

992 5. Kim EB, Fang X, Fushan AA, Huang Z, Lobanov A V., Han L, et al. Genome
993 sequencing reveals insights into physiology and longevity of the naked mole rat.
994 Nature. 2011;479: 223–227. doi:10.1038/nature10533

995 6. Fang X, Seim I, Huang Z, Gerashchenko M V., Xiong Z, Turanov AA, et al.
996 Adaptations to a Subterranean Environment and Longevity Revealed by the
997 Analysis of Mole Rat Genomes. Cell Rep. 2014;8: 1354–1364.
998 doi:10.1016/j.celrep.2014.07.030

999 7. Yu C, Li Y, Holmes A, Szafranski K, Faulkes CG, Coen CW, et al. RNA sequencing
1000 reveals differential expression of mitochondrial and oxidation reduction genes in
1001 the long-lived naked mole-rat when compared to mice. PLoS One. Public Library
1002 of Science; 2011;6: e26729. doi:10.1371/journal.pone.0026729

1003 8. Pérez VI, Buffenstein R, Masamsetti V, Leonard S, Salmon AB, Mele J, et al. Protein
1004 stability and resistance to oxidative stress are determinants of longevity in the
1005 longest-living rodent, the naked mole-rat. Proc Natl Acad Sci U S A. 2009;106:
1006 3059–64. doi:10.1073/pnas.0809620106

1007 9. Rodriguez KA, Edrey YH, Osmulski P, Gaczynska M, Buffenstein R. Altered
1008 composition of liver proteasome assemblies contributes to enhanced proteasome
1009 activity in the exceptionally long-lived naked mole-rat. PLoS One. Public Library
1010 of Science; 2012;7: e35890. doi:10.1371/journal.pone.0035890

1011 10. Buffenstein R. Negligible senescence in the longest living rodent, the naked mole-
1012 rat: Insights from a successfully aging species [Internet]. Journal of Comparative
1013 Physiology B: Biochemical, Systemic, and Environmental Physiology. 2008. pp.
1014 439–445. doi:10.1007/s00360-007-0237-5

1015 11. Lewis KN, Wason E, Edrey YH, Kristan DM, Nevo E, Buffenstein R. Regulation of
1016 Nrf2 signaling and longevity in naturally long-lived rodents. Proc Natl Acad Sci U
1017 S A. National Academy of Sciences; 2015;112: 3722–7.
1018 doi:10.1073/pnas.1417566112

1019 12. Tian X, Azpurua J, Hine C, Vaidya A, Myakishev-Rempel M, Ablaeva J, et al. High-
1020 molecular-mass hyaluronan mediates the cancer resistance of the naked mole rat.
1021 Nature. 2013;499: 346–349. doi:10.1038/nature12234

1022 13. Andziak B, O'Connor TP, Qi W, DeWaal EM, Pierce A, Chaudhuri AR, et al. High
1023 oxidative damage levels in the longest-living rodent, the naked mole-rat. Aging
1024 Cell. 2006;5: 463–471. doi:10.1111/j.1474-9726.2006.00237.x

1025 14. Holtze S, Eldarov CM, Vays VB, Vangeli IM, Vysokikh MY, Bakeeva LE, et al. Study
1026 of age-dependent structural and functional changes of mitochondria in skeletal
1027 muscles and heart of naked mole rats (Heterocephalus glaber). Biochem.

1028 2016;81: 1429–1437. doi:10.1134/S000629791612004X
1029 15. Lewis KN, Andziak B, Yang T, Buffenstein R. The naked mole-rat response to
1030 oxidative stress: just deal with it. Antioxid Redox Signal. Mary Ann Liebert, Inc.;
1031 2013;19: 1388–99. doi:10.1089/ars.2012.4911
1032 16. Finkel T. The metabolic regulation of aging. Nat Med. 2015;21: 1416–1423.
1033 doi:10.1038/nm.3998
1034 17. Fontana L, Partridge L. Promoting Health and Longevity through Diet: From
1035 Model Organisms to Humans. Cell. 2015;161: 106–118.
1036 doi:10.1016/j.cell.2015.02.020
1037 18. Davinelli S, Willcox DC, Scapagnini G. Extending healthy ageing: nutrient sensitive
1038 pathway and centenarian population. Immun Ageing. 2012;9: 9.
1039 doi:10.1186/1742-4933-9-9
1040 19. Sahm A, Bens M, Platzer M, Cellerino A. Parallel evolution of genes controlling
1041 mitonuclear balance in short-lived annual fishes. Aging Cell. 11 Feb 2017.
1042 doi:10.1111/acel.12577
1043 20. Houtkooper RH, Mouchiroud L, Ryu D, Moullan N, Katsyuba E, Knott G, et al.
1044 Mitonuclear protein imbalance as a conserved longevity mechanism. Nature.
1045 Nature Publishing Group, a division of Macmillan Publishers Limited. All Rights
1046 Reserved.; 2013;497: 451–7. doi:10.1038/nature12188
1047 21. Brandt T, Mourier A, Tain LS, Partridge L, Larsson N-G, Kühlbrandt W. Changes of
1048 mitochondrial ultrastructure and function during ageing in mice and Drosophila.
1049 Elife. 2017;6. doi:10.7554/eLife.24662
1050 22. Park TJ, Reznick J, Peterson BL, Blass G, Omerbašić D, Bennett NC, et al. Fructose-
1051 driven glycolysis supports anoxia resistance in the naked mole-rat. Science (80-).
1052 2017;356: 307–311. doi:10.1126/science.aab3896
1053 23. Ori A, Toyama BH, Harris MS, Bock T, Iskar M, Bork P, et al. Integrated
1054 Transcriptome and Proteome Analyses Reveal Organ-Specific Proteome
1055 Deterioration in Old Rats. Cell Syst. Elsevier; 2015;1: 224–237.
1056 doi:10.1016/j.cels.2015.08.012
1057 24. Schwanhäusser B, Busse D, Li N, Dittmar G, Schuchhardt J, Wolf J, et al. Global
1058 quantification of mammalian gene expression control. Nature. Nature Publishing
1059 Group, a division of Macmillan Publishers Limited. All Rights Reserved.;
1060 2011;473: 337–42. doi:10.1038/nature10098
1061 25. Vogel C, Marcotte EM. Insights into the regulation of protein abundance from
1062 proteomic and transcriptomic analyses. Nat Rev Genet. 2012;13: 227–32.
1063 doi:10.1038/nrg3185
1064 26. Nyström T, Yang J, Molin M. Peroxiredoxins, gerontogenes linking aging to
1065 genome instability and cancer. Genes Dev. 2012;26: 2001–8.
1066 doi:10.1101/gad.200006.112
1067 27. Hanzén S, Vielfort K, Yang J, Roger F, Andersson V, Zamarbide-Forés S, et al.
1068 Lifespan Control by Redox-Dependent Recruitment of Chaperones to Misfolded
1069 Proteins. Cell. Elsevier; 2016;166: 140–151. doi:10.1016/j.cell.2016.05.006
1070 28. Biteau B, Karpac J, Supoyo S, DeGennaro M, Lehmann R, Jasper H. Lifespan
1071 extension by preserving proliferative homeostasis in Drosophila. Kim SK, editor.
1072 PLoS Genet. Public Library of Science; 2010;6: 1–15.
1073 doi:10.1371/journal.pgen.1001159
1074 29. Erol A. The Functions of PPARs in Aging and Longevity. PPAR Res. Hindawi;
1075 2007;2007: 39654. doi:10.1155/2007/39654
1076 30. Bustos V, Partridge L. Good Ol' Fat: Links between Lipid Signaling and Longevity.
1077 Trends Biochem Sci. 2017; doi:10.1016/j.tibs.2017.07.001

1078 31. Cellerino A, Ori A. What have we learned on aging from omics studies? Semin Cell
1079 Dev Biol. 2017; doi:10.1016/j.semcdb.2017.06.012
1080 32. Delire B, Lebrun V, Selvais C, Henriet P, Bertrand A, Horsmans Y, et al. Aging
1081 enhances liver fibrotic response in mice through hampering extracellular matrix
1082 remodeling. Aging (Albany NY). Impact Journals, LLC; 2016;9: 98–113.
1083 doi:10.18632/aging.101124
1084 33. Hattori K, Inoue M, Inoue T, Arai H, Tamura H. A novel sulfotransferase
1085 abundantly expressed in the dauer larvae of Caenorhabditis elegans. J Biochem.
1086 2006;139: 355–62. doi:10.1093/jb/mvj041
1087 34. Fielenbach N, Antebi A. C. elegans dauer formation and the molecular basis of
1088 plasticity. Genes Dev. 2008;22: 2149–65. doi:10.1101/gad.1701508
1089 35. Murphy CT, McCarroll SA, Bargmann CI, Fraser A, Kamath RS, Ahringer J, et al.
1090 Genes that act downstream of DAF-16 to influence the lifespan of Caenorhabditis
1091 elegans. Nature. 2003;424: 277–83. doi:10.1038/nature01789
1092 36. White RR, Milholland B, MacRae SL, Lin M, Zheng D, Vijg J. Comprehensive
1093 transcriptional landscape of aging mouse liver. BMC Genomics. BioMed Central;
1094 2015;16: 899. doi:10.1186/s12864-015-2061-8
1095 37. Durieux J, Wolff S, Dillin A. The cell-non-autonomous nature of electron transport
1096 chain-mediated longevity. Cell. 2011;144: 79–91. doi:10.1016/j.cell.2010.12.016
1097 38. Baumgart M, Priebe S, Groth M, Hartmann N, Menzel U, Pandolfini L, et al.
1098 Longitudinal RNA-seq analysis of vertebrate aging identifies mitochondrial
1099 complex i as a small-molecule-sensitive modifier of lifespan. Cell Syst. 2016;2:
1100 122–132. doi:10.1016/j.cels.2016.01.014
1101 39. Miwa S, Jow H, Baty K, Johnson A, Czapiewski R, Saretzki G, et al. Low abundance
1102 of the matrix arm of complex I in mitochondria predicts longevity in mice. Nat
1103 Commun. Nature Publishing Group; 2014;5: 3837. doi:10.1038/ncomms4837
1104 40. Sgarbi G, Matarrese P, Pinti M, Lanzarini C, Ascione B, Gibellini L, et al.
1105 Mitochondria hyperfusion and elevated autophagic activity are key mechanisms
1106 for cellular bioenergetic preservation in centenarians. Aging (Albany NY). Impact
1107 Journals, LLC; 2014;6: 296–310. doi:10.18632/aging.100654
1108 41. Sengupta S, Peterson TR, Laplante M, Oh S, Sabatini DM. mTORC1 controls
1109 fasting-induced ketogenesis and its modulation by ageing. Nature. Nature
1110 Research; 2010;468: 1100–1104. doi:10.1038/nature09584
1111 42. Luis NM, Wang L, Ortega M, Deng H, Katewa SD, Li PW-L, et al. Intestinal IRE1 Is
1112 Required for Increased Triglyceride Metabolism and Longer Lifespan under
1113 Dietary Restriction. Cell Rep. Elsevier; 2016;17: 1207–1216.
1114 doi:10.1016/j.celrep.2016.10.003
1115 43. Mitchell SJ, Madrigal-Matute J, Scheibye-Knudsen M, Fang E, Aon M, González-
1116 Reyes JA, et al. Effects of Sex, Strain, and Energy Intake on Hallmarks of Aging in
1117 Mice. Cell Metab. Elsevier; 2016;23: 1093–1112. doi:10.1016/j.cmet.2016.05.027
1118 44. Hahn O, Grönke S, Stubbs TM, Ficz G, Hendrich O, Krueger F, et al. Dietary
1119 restriction protects from age-associated DNA methylation and induces epigenetic
1120 reprogramming of lipid metabolism. Genome Biol. 2017;18: 1194.
1121 doi:10.1186/s13059-017-1187-1
1122 45. Kim HE, Grant AR, Simic MS, Kohnz RA, Nomura DK, Durieux J, et al. Lipid
1123 Biosynthesis Coordinates a Mitochondrial-to-Cytosolic Stress Response. Cell.
1124 2016;166: 1539–1552.e16. doi:10.1016/j.cell.2016.08.027
1125 46. Weir HJ, Yao P, Huynh FK, Escoubas CC, Goncalves RL, Burkewitz K, et al. Dietary
1126 Restriction and AMPK Increase Lifespan via Mitochondrial Network and
1127 Peroxisome Remodeling. Cell Metab. 2017; doi:10.1016/j.cmet.2017.09.024

1128 47. Toth M, Tchernof A. Lipid metabolism in the elderly. Eur J Clin Nutr. Nature
1129 Publishing Group; 2000;54: S121–S125. doi:10.1038/sj.ejcn.1601033
1130 48. Solomon TPJ, Marchetti CM, Krishnan RK, Gonzalez F, Kirwan JP. Effects of aging
1131 on basal fat oxidation in obese humans. Metabolism. 2008;57: 1141–1147.
1132 doi:10.1016/j.metabol.2008.03.021
1133 49. St-Onge M-P, Gallagher D. Body composition changes with aging: the cause or the
1134 result of alterations in metabolic rate and macronutrient oxidation? Nutrition.
1135 NIH Public Access; 2010;26: 152–5. doi:10.1016/j.nut.2009.07.004
1136 50. Franceschi C, Campisi J, LR M, J C, JL K, HY C. Chronic Inflammation
1137 (Inflammaging) and Its Potential Contribution to Age-Associated Diseases.
1138 Journals Gerontol Ser A Biol Sci Med Sci. Oxford University Press; 2014;69: S4–S9.
1139 doi:10.1093/gerona/glu057
1140 51. Done AJ, Gage MJ, Nieto NC, Traustadóttir T. Exercise-induced Nrf2-signaling is
1141 impaired in aging. Free Radic Biol Med. 2016;96: 130–138.
1142 doi:10.1016/j.freeradbiomed.2016.04.024
1143 52. Safdar A, deBeer J, Tarnopolsky MA. Dysfunctional Nrf2–Keap1 redox signaling in
1144 skeletal muscle of the sedentary old. Free Radic Biol Med. 2010;49: 1487–1493.
1145 doi:10.1016/j.freeradbiomed.2010.08.010
1146 53. Bens M, Szafranski K, Holtze S, Sahm A, Groth M, Kestler HA, et al. Naked mole-rat
1147 transcriptome signatures of socially-suppressed sexual maturation and links of
1148 reproduction to aging. bioRxiv. Cold Spring Harbor Laboratory; 2017; 221333.
1149 doi:10.1101/221333
1150 54. Buffenstein R, Jarvis JUM. The Naked Mole Rat--A New Record for the Oldest
1151 Living Rodent. Sci Aging Knowl Environ. 2002;2002: 7pe–7.
1152 doi:10.1126/sageke.2002.21.pe7
1153 55. Dammann P, Šumbera R, Maßmann C, Scherag A, Burda H. Extended Longevity of
1154 Reproductives Appears to be Common in Fukomys Mole-Rats (Rodentia,
1155 Bathyergidae). de Polavieja GG, editor. PLoS One. 2011;6: e18757.
1156 doi:10.1371/journal.pone.0018757
1157 56. Dammann P, Burda H. Sexual activity and reproduction delay ageing in a
1158 mammal. Curr Biol. 2006;16: R117–R118. doi:10.1016/j.cub.2006.02.012
1159 57. Bens M, Sahm A, Groth M, Jahn N, Morhart M, Holtze S, et al. FRAMA: from RNA-
1160 seq data to annotated mRNA assemblies. BMC Genomics. 2016;17: 54.
1161 doi:10.1186/s12864-015-2349-8
1162 58. Sahm A, Bens M, Platzer M, Szafranski K. PosiGene: automated and easy-to-use
1163 pipeline for genome-wide detection of positively selected genes. Nucleic Acids
1164 Res. 2017;45: e100–e100. doi:10.1093/nar/gkx179
1165 59. Hughes CS, Foehr S, Garfield DA, Furlong EE, Steinmetz LM, Krijgsveld J.
1166 Ultrasensitive proteome analysis using paramagnetic bead technology. Mol Syst
1167 Biol. 2014;10: 757. Available:
1168 http://www.pubmedcentral.nih.gov/articlerender.fcgi?artid=4299378&tool=pm
1169 centrez&rendertype=abstract
1170 60. Cox J, Neuhauser N, Michalski A, Scheltema RA, Olsen J V., Mann M. Andromeda: A
1171 Peptide Search Engine Integrated into the MaxQuant Environment. J Proteome
1172 Res. 2011;10: 1794–1805. doi:10.1021/pr101065j
1173 61. Cox J, Mann M. MaxQuant enables high peptide identification rates, individualized
1174 p.p.b.-range mass accuracies and proteome-wide protein quantification. Nat
1175 Biotechnol. 2008;26: 1367–72. doi:10.1038/nbt.1511
1176 62. Elias JE, Gygi SP. Target-decoy search strategy for increased confidence in large-
1177 scale protein identifications by mass spectrometry. Nat Methods. 2007;4: 207–

1178 214. doi:10.1038/nmeth1019

1179 63. Ritchie ME, Phipson B, Wu D, Hu Y, Law CW, Shi W, et al. limma powers
1180 differential expression analyses for RNA-sequencing and microarray studies.
1181 Nucleic Acids Res. 2015;43: e47–e47. doi:10.1093/nar/gkv007

1182 64. Benjamini Y, Hochberg Y. Controlling the False Discovery Rate: A Practical and
1183 Powerful Approach to Multiple Testing [Internet]. Journal of the Royal Statistical
1184 Society. Series B (Methodological). WileyRoyal Statistical Society; 1995. pp. 289–
1185 300. doi:10.2307/2346101

1186 65. Brosch M, Yu L, Hubbard T, Choudhary J. Accurate and sensitive peptide
1187 identification with Mascot Percolator. J Proteome Res. 2009;8: 3176–81.
1188 doi:10.1021/pr800982s

1189 66. Gatto L, Lilley KS. MSnbase-an R/Bioconductor package for isobaric tagged mass
1190 spectrometry data visualization, processing and quantitation. Bioinformatics.
1191 2012;28: 288–289. doi:10.1093/bioinformatics/btr645

1192 67. Huber W, von Heydebreck A, Sültmann H, Poustka A, Vingron M. Variance
1193 stabilization applied to microarray data calibration and to the quantification of
1194 differential expression. Bioinformatics. 2002;18 Suppl 1: S96-104.

1195 68. Bruderer R, Bernhardt OM, Gandhi T, Miladinović SM, Cheng L-Y, Messner S, et al.
1196 Extending the limits of quantitative proteome profiling with data-independent
1197 acquisition and application to acetaminophen-treated three-dimensional liver
1198 microtissues. Mol Cell Proteomics. 2015;14: 1400–10.
1199 doi:10.1074/mcp.M114.044305

1200 69. Storey JD. A direct approach to false discovery rates. J R Stat Soc Ser B (Statistical
1201 Methodol. Blackwell Publishers; 2002;64: 479–498. doi:10.1111/1467-
1202 9868.00346

1203 70. Luo W, Friedman MS, Shedden K, Hankenson KD, Woolf PJ. GAGE: generally
1204 applicable gene set enrichment for pathway analysis. BMC Bioinformatics.
1205 2009;10: 161. doi:10.1186/1471-2105-10-161

1206 71. Subramanian A, Tamayo P, Mootha VK, Mukherjee S, Ebert BL, Gillette MA, et al.
1207 Gene set enrichment analysis: a knowledge-based approach for interpreting
1208 genome-wide expression profiles. Proc Natl Acad Sci U S A. National Academy of
1209 Sciences; 2005;102: 15545–50. doi:10.1073/pnas.0506580102

1210 72. Supek F, Bošnjak M, Škunca N, Šmuc T. REVIGO summarizes and visualizes long
1211 lists of gene ontology terms. PLoS One. Public Library of Science; 2011;6: e21800.
1212 doi:10.1371/journal.pone.0021800

1213